Article Type: Research Article

Corresponding Author Email ID: adgcal@gmail.com

Medical Devices and Sensors

Medical Devices and Sensors ISSUE: PAGEX-PAGEy (20xx)
Published online XX Month 20xx in Wiley Online Library
(wileyonlinelibrary.com) DOI: XX.XXXX/XXX.XXX

Bioelectronics At Graphene Biofilm Interface: Schottky junction formation and capacitive transitions

Sanhita Ray[1], Sayantani Sen[2], Alakananda Das[2], Anirban Bose[1], Anirban Bhattacharyya[2], Avishek Das[3], Sanatan Chattopadhyay[3], Shib Shankar Singha[4]

Achintya Singha[4], Hirak K. Patra[5] and Anjan Kr. Dasgupta[1,†]

[1,†]Department of Biochemistry, University of Calcutta, Kolkata, India

[2] Institute of Radiophysics and Electronics, University of Calcutta, Kolkata, India

[3] Department of Electronic Science, University of Calcutta, Kolkata, India

[4] Department of Physics, Bose Institute, Kolkata, India

[5] Department of Chemical Engineering and Biotechnology, University of Cambridge, United Kingdom

ABSTRACT

We have used an interface of bacterial community and graphene that may provide a platform for tunable bioelectronic components. Graphene nanoplatelets were immobilized by using the establishment process of photosynthetic, purple non-sulphur biofilm. While immobilized on metallic electrodes, DC current-voltage plot exhibited symmetric threshold voltage which is indicative of both-way Schottky diode formation. When immobilization was allowed to take place on metallic electrodes, DC current-voltage plot exhibited symmetric threshold voltage. This was indicative of both way Schottky diode formation. The biomaterial itself demonstrated presence of convergence points in capacitive spectra on frequency axis, when AC amplitude was varied. Incorporation of

graphene disrupted such points of convergence and increase the photo-pigment content in biofilms in response to it. Limiting the carbon source was found to diminish and ultimately reverse this effect. In summary, cross-talk between the surface electron cloud of two dimensional (2D) graphene and biofilm, growing on a 2D surface, can lead to smart hybrid materials, which in turn can be exploited as bioelectronic components.

KEY WORDS:Graphene; Immobilization; Photosynthetic biofilm; Schottky diode; Capacitance

Received: April 2018

Accepted: not yet

1 Introduction

The advanced functional properties of biomaterial biofilm [1, 2, 3] and 2D material graphene [4, 5, 6] are remarkable but there are only limited reports on the cross-talk and synergy of the functions of these two classes of materials. In most cases, one attempts to use graphene as a negative regulator of biofilm growth[7]. This approach is closely related to the perception that biofilms are formed by pathogenic bacteria. However if we consider biofilm of photosynthetic bacteria one may not be keen to suppress its growth. On the other hand there may be a beneficial exploitation such as [8] if we can further the stabilization of such films as it may be useful as a photon capture or even as a sensor device.

Graphene immobilization has been achieved previously by adding soluble graphene oxide (GO) to growing cultures of biofilm-forming microbial species. Microbial cultures typically achieve reduction of GO [9, 10, 11, 12, 13] and form reduced graphene oxide (RGO). Both GO and RGO have much higher defect densities compared to pristine graphene. We have aimed an alternate approach: to achieve immobilization of graphene nanoplatelets obtained from chemical vapour deposition (CVD). CVD synthesized graphene has lower defect densities and higher conductivity [14] compared to both RGO and GO. CVD graphene is also comparatively more hydrophobic.

Biofilm is emerging as systemic biomaterials that could potentially help in the development of future living electronics. Earlier reports on RGO incorporated into biofilms resulted in increased conductivity of microbial fuel cells (MFC) and bio-photovoltaic cells (BPV) [9, 10, 11, 12, 13]. Together with recent findings of conducting nanowires in Geobacter [15], as well as hybrid CdS bacteria solar power mining [16], indicating the feasibility of biofilm-based electronics in near future realization [16].

Typically, semiconducting materials possess an energy barrier or band gap (V_B) between their valence electrons (closely bound) and conduction band (consisting of free electrons). Valence band electrons must be supplied with $energy > V_B$ for a transition to the conduction band. A tight contact may be obtained between a metal (M) and semiconductor(S), such that charge may flow from one to the other. Such a junction gives rise to a Schottky diode having a signature threshold voltage (V_B) [17, 18]. Current flow occurs only for voltages $V > V_B$. Graphene-based Schottky diodes typically involve graphene (metal)- silicon (semiconductor) junction.

To track the changes in the electrical properties of the biofilm in the presence and absence of graphene we have explored frequency dependent capacitance change. Capacitance (C) of biofilms is related to its charge storing ability. Many biological components contribute to charge storage e.g. proteins, polar head groups of lipids, chromophores, pigments etc. How interaction with graphene changes capacitance would reveal the nature of possible interactions the biofilm may have with the graphene. Changes in capacitance (C) and impedance (G) [19, 20, 21, 22] are measured by applying sinusoidally oscillating voltage. G and C values are obtained as a function of the frequency of oscillation.

The principal aim of this present work is to develop and demonstrate the potential use of conductive biofilms in future bioelectronic devices. The report demonstrated here as the first study of this kind where direct DC conductivity and capacitance, as a function of frequency, for graphene incorporated biofilms.

2 Results

2.1 Graphene immobilization

Graphene nanoplatelets were added to the growth medium (RCV, see Figure 2) for photosynthetic biofilm-forming bacteria, *Rhodobacter capsulatus*. Graphene flakes were immobilized within the biofilm, during growth of the biofilm. For measurement of electrical properties, graphene incorporated biofilm was grown on interdigitated electrodes.

2.2 Electron microscopy

Graphene immobilization was observed in scanning electron microscopic images (see Figure 3(a, control and b, graphene incorporated)) of 11th-day old graphene incorporated biofilms. Since 11th-day biofilms are quite old (mature biofilms occur at the 4th-7th day of

growth), they show considerable sloughing. As a result, wrinkled platelets (see Figure 3(b), yellow arrows) of graphene are clearly visible, trapped underneath a network of biofilm cells (with a smooth surface, see Figure 3(b), red arrows).

Figure 3(c) and (d) show light microscopic images of control and graphene incorporated biofilm grown on interdigitated electrode (IDE) surface.

2.3 Raman characterization

Raman spectra of biofilm incorporated graphene could not be obtained. Raman signal from carbohydrates (see supplementary figure S4) masked the Raman signature of graphene. This is proof that graphene was effectively trapped within extra-cellular polysaccharide so that its surface is not accessible to light.

Raman spectrum was obtained for the graphene that was used for this study. Raman spectrum (figure 4) obtained with red laser (632 nm) showed $I_D : I_G$ ratio of 1.259 and using the relation of this ratio to average distance between defects (L_D) as in Cancado et al [23], L_D was determined to be 15.194 nm, which is greater than the average L_D for RGO which is around 3-4 nm [24, 14]. Hence our sample had relatively fewer defects compared to RGO and hence of higher hydrophobicity. Hydrophobicity is the important parameter that prevents interaction of graphene [25] with most aqueous-based biosystems.

The anomalous hump like 2D peak has been reported for few-layer wrinkled graphenes [26] (FlWG), hence we may infer a part of the used graphene to contain FlWG. This is supported by the abnormally high FWHM of our samples of 65 cm^{-1} (G band) and 52 cm^{-1} (D band), as previously reported. In addition, the high intensity (almost same as I_G) around 2D region suggests decoration of wrinkled forms on the surface of larger sheets (since FlWG does not have as high 2D) and is supported by the SEM images of trapped sheets (supplementary figure S2). Raman spectra of used graphene are important since FlWG are known to possess an intrinsic band gap in many cases.

The wrinkled nature is supported by another Raman spectrum obtained with 488 nm laser, which shows an average distance between the defect of 10 nm (see supplementary figure S3) yet the distance between edges of 4.358 nm (according to Tunistra-Koenig relation). Wrinkling and folding may be responsible for reducing the size by bringing the edges much closer to each other and increasing the effective defect density. Please note that due to repetitive folding, sheet-like structure is modified into platelets or particulate matter.

2.4 Biofilm characterization and effects on biofilm metabolism

Biofilms were characterized by standard methods like pigment estimation (since Rhodobacter is photosynthetic) and crystal violet assay (see Figure 5(a-b)). Measurements of pigment concentration (see Figure 5 (a) and (c)) in Rhodobacter biofilms demonstrated the effects of graphene incorporation on photosynthetic machinery as well as other metabolic processes (e.g. carbon metabolism). Stain retention assays (see Figure 5 (b)) are a standardized method for determining biofilm biomass and shows the effect of graphene incorporation.

Photopigment concentration in biofilms was estimated by measuring the absorbance of organic extract (sup, in chloroform-ethanol 1:4 mixture) from biofilms. The procedure used here for extracting photopigments does not disrupt the biofilm physically and hence there is no graphene present in this sup (confirmed by centrifuging the extract, no graphene pellets observed). Absorbance spectra of organic extract (see SUPPLEMENTARY figure S5) showed peaks corresponding to various light-harvesting complexes (LHC). Pigment corresponding to absorption at 370 nm was studied over 4 days of biofilm growth.

Figure 5a showed increased pigment concentration in Rhodobacter biofilms upon graphene incorporation. Over a period of 2-4 days of biofilm growth, the pigment content of graphene incorporated biofilms increased at a rate higher than that of control biofilms.

For increasing concentrations of graphene, the sup exhibited a higher concentration of photopigments in the biofilm (see figure 5(b, inset) and supplementary figures S6 and S7).

Growth of photosynthetic biofilm in presence of graphene was confirmed by performing crystal violet (CV) staining assay (see Figure 5(b)). CV staining gives an estimate of biofilm biomass. CV staining showed that biofilm biomass increased with increasing concentrations of graphene in bacterial growth media, but decreased for the highest dose of graphene (5.5 mg in 50 ml media). Effect of incorporated graphene on CV staining was negligible since biofilm consisted of much more organic biomass compared to amount of incorporated graphene (since most of added graphene can be recovered from the used growth medium and reused).

Sub-optimal concentrations of malic acid (4 mg/ml), the primary organic carbon source in growth medium was used to test relationship of this pigment enhancement effect with carbon metabolism in *Rhodobacter*. Photopigment enhancement, in presence of graphene, was much lower for lesser concentrations of malic acid (see Figure 5(c)). When no malic acid was added to growth medium, presence of graphene resulted in decreased pigmentation. Regulatory systems governing photopigment concentration are therefore responsive to organic carbon source availibility. Pigment concentrations are increased in presence of graphene only when sufficient malic acid is available.

Rhodobacter capsulatus strain has been shown to exhibit fluorescence [27] at 613 nm upon excitation at 395 nm. Hence absorbance of planktonic fraction was studied at 392 nm (supplementary Figure S6(a)), when malic acid was withdrawn, in presence and absence of graphene. Absorption by photopigments in planktonic fraction was higher when graphene was present. While graphene in all cases partially quenched the fluorescence , the increase in fluorescence with increasing malic acid concentration had a steeper slope when graphene was present (supplementary Figure S6(b-c)). Hence the role of graphene has been to alter the photochemistry in the membrane of *Rhodobacter*. This points towards interaction between Dirac Fermions on the surface of graphene and the pigments associated with light energy harvesting in the purple non-sulphur bacteria. All the consequent emergent properties can be linked to this superposition of electron clouds.

2.5 Biodiode characterization

Current-voltage (IV) curves for control and graphene incorporated biofilms (see Figure 6(a)) were obtained by applying varying DC voltage across a two electrode system (see Figure 2(c-f)). Control biofilm showed a current of the order of $10^{-11}A$ and significant hysteretic properties (see Supplementary Figure S9(a)). IV curve for biofilms grown with 4.4 mg graphene in 50 ml media (g4, see Figure 6(a)) showed the presence of a critical or threshold voltage (Figure 6(a)) at $\pm 3.2V$. Below this threshold, the current through the bio-composite was of the order of $10^{-7}A$. Above the threshold voltage, current increased sharply from $10^{-7}A$ to $5X10^{-3}A$. For higher dose of graphene (g4), this threshold was symmetric, i.e. present for both positive and negative voltages. When the voltage was stepped up from zero to higher (positive or negative) values, a hump appeared in the IV curve, immediately following the threshold voltage.

Conductance (see Figure 6(b)) of biocomposites was obtained as the gradient of current against voltage and plotted for corresponding voltage values. Conductance showed a sharp increase above the threshold voltage. Hump in IV curve was translated into a well-defined conductance peak at ±3.3 V. Presence of conductance peak indicates tunneling current between graphene islands located in close proximity. It is to be noted that we are studying the emergent electrical properties of a complex material consisting water, suspended biopolymers and cells, dissolved ions as well as entrapped conductor, i.e. graphene.

When the dose of graphene was lesser (2 mg in 50 ml media, g2), threshold was observed in only one direction (see Figure 7). This indicates that because of lesser quantities of graphene present in the medium, diode junction was formed only on one electrode. This provides further proof that indeed a diode junction was responsible for the observed properties. For this lower dose of graphene, the biocomposite showed overall lesser current conduction (of the range of $10^{-6}A$, see supplementary Figure S9). Across a particular range of voltage values, we obtained a current in the opposite direction with

respect to applied voltage i.e. negative conductance. This is the hallmark of capacitive current and is attributable to higher proportion of insulating biomaterial.

The threshold voltage in an I-V curve, followed by a steep rise in conductance generally indicates formation of a diode junction.. Diode junctions are formed when there is charge flow between two types of semiconductors or from semiconductor to metal. At room temperature, graphene has zero band gap, i.e. it behaves as a metal. However strain induction is known to cause opening up of band gap in suitably functionalized graphene. Hence we may infer that Schottky junction has been formed between strained entrapped graphene (semiconductor) and gold layer (metal). Thus, threshold voltage in IV curve corresponds to the diode threshold. This result demonstrates the role of biofilm in engineering the band gap of a 2D material.

2.6 Capacitive properties

Capacitive properties of graphene-biofilm composite were measured by applying an AC voltage across a two electrode system with 20 μm (IDE2, see Methods). Capacitance values were obtained as a function of frequency. Capacitance spectrum, on frequency axis, changed when amplitude or root mean square (RMS), of applied AC voltage, was changed. Effect of RMS voltage change on biomaterials capacitance is studied here for the first time.

For control biofilm (see figure 8(a)), i.e. in the absence of graphene, capacitance spectra showed points of convergence at frequencies 0.9 and 6 MHz. We refer to these points of convergence as isosbestic points. Isosbestic points divided the capacitance spectrum into two sections: on one side capacitance values increased with increasing RMS values, but decreased with increasing RMS on the other side.

For graphene incorporated biofilms (see figure 8(b)), clear convergence point could not be obtained. In fact, capacitance values showed high standard deviation specifically at and around the isosbestic point. This implies that graphene associates with dielectric components present in the membrane and changes their response to electric field. The component of biofilm most likely to change their alignment in the presence of graphene are the planar photopigments. This corresponds well with the effect of graphene on photopigment concentration in biofilms.

Isosbestic points are commonly observed in spectrophotometry. When an interspecies conversion is studied by spectrophotometry or fluorometry, two peaks usually occur corresponding to the two species. As the reaction progresses, successive spectra show change in peak ratio as well as a convergence point for all spectra. This convergence point

is referred to as isosbestic point by spectroscopists and we have borrowed the term in our case. Presence of an isosbestic point signifies direct conversion of one species into another, without the presence of any intermediate.

In case of capacitance spectra, isosbestic point implies conversion of one dielectric into another or more likely, a state change in a dielectric, following change in amplitude of applied AC voltage. The first species shows highest dielectric alignment below 0.9 MHz and above 6 MHz, when RMS voltage is low. The second species shows highest alignment for a comparatively narrower band of frequencies between the two isosbestic points.

All the above effects are systems level, emergent properties that hint towards specific molecular level interaction between graphene and specific components of biofilms. FTIR spectra (see Figure S11) offers us a brief glimpse into such interaction. Notably, the C=C bond intensity in graphene powder is increased manifold when graphene was incorporated into biofilm. This indicates that graphene is "biologically exfoliated" and dispersed during the process of incorporation. Another source of information on molecular interactions between biofilm and graphene can be derived from NIR spectra (see Figure S12) from aqueous suspensions of graphene-biofilm composite. The results show that graphene predominantly interacts with 3 components and we suggest the mechanisms for the following: lipids (hydrophobic collapse), bacteriochlorophyll (stacking interaction) and water (water exclusion).

3 Discussions

The fact that biofilms possess interesting material properties [28] is often masked by the huge literature describing the dangers posed by biofilms from pathogenic bacteria. The literature of biofilms is thus dominated by the search for agents that destabilizes biofilms. The graphene biofilm interaction studies reported earlier are no exception [29], as most of such studies are devoted to using of graphene as inhibitor of pathogenic biofilm.

The biofilms of photosynthetic bacteria are non-pathogenic and eco-friendly. This paper shows how a near 2D, photon capturing system interacts [30, 31, 32] with a Dirac-2D material (graphene). We describe some interesting electrical properties (see supplementary Figure S13) of such hybrid nano-biomaterial, where graphene is trapped within a photosynthetic biofilm. What emerges is a new platform for bandgap engineering where semiconductor-like properties can emerge by interfacing photosynthetic biofilms with graphene. We however need to explore whether the building blocks of the biofilm or the pigments therein are primarily responsible for emergence of new electrical properties (altered band gap) (see supplementary Figure S14).

The focus of this study is on the interface that develops between inorganic graphene and a biological entity i.e. biofilm. Systems level, emergent electrical properties have been experimentally demonstrated. This leaves open the question of molecular level interactions for further studies.

The problem is made non-trivial due to the complex nature of biofilms, especially photosynthetic biofilms, containing numerous chemical entities with whom graphene may interact. There are a few promising candidates: carbohydrates (as in extracellular polysaccharides (EPS)), lipids in outer membrane as well as photosynthetic machinery including light harvesting pigments. Navigation through such a complex system can only be achieved (at least initially) by using a detailed simulations approach [33, 34]. It may not be possible to isolate each and every component and perform experiments by exactly mimicking the biofilm internal mileau. Simulations approach would allow us to explore such organic-inorganic interfaces at various scales: at the macroscale using coarse grained approaches, at the nanoscale by using molecular dynamics simulations and at the level of electrons by using quantum mechanical approaches. This last component is especially important in case of graphene since it is a Dirac material having a cloud of massless Fermions on its surface which is expected to show interactions with photosynthetic machinery where the tunneling of electrons is a widely studied quantum mechanical phenomenon.

One previous molecular dynamics study [35, 36] has shown correlation between defect density of graphene and behaviour of lipid membrane in presence of various types of graphene. This study is important for predicting effect of various types of graphene on bacteria that possess an outer membrane. The lipid composition of such outer membranes is also important.

Few layer graphene with very little point defects were intercalated between hydrophobic tails of phospholipids without disrupting the membrane. Graphene oxide (bearing charged functional groups) showed interaction with polar head groups of membrane lipids resulting in lipid extrac-
tion.

Hence the general conclusion from simulation studies is that higher defect density (hydrophilic) leads to disruption of membrane structure whereas more pristine forms of graphene (hydrophobic) are harmlessly integrated into lipid structures. Relating these findings with more detailed experimental findings is the topic for an upcoming publication we are currently working on.

Graphene nanoplatelets are a cheap form of graphene which nevertheless has higher conductivity compared to RGO. However, immobilization of such powdered forms is quite difficult and hence costly. We present a cheap, green method for immobilizing graphene powder using a photosynthetic microbe. We have reported the correlation between

changes in conductive and dielectric properties of the biofilm with a change in photopigment concentration and fluorescence properties.

Electrical characterization with DC voltage has brought to light a novel application for graphene immobilization. IV curve for graphene incorporated biofilm showed evidence for diode junction formation at gold electrodes. This proves that biofilm growth is capable of engineering the band gap of graphene. Hence we may extend this principle to engineering the band gap of other 2D materials with intrinsic band gap (e.g. MoS2, WS2). Such materials can become the basis for green electronics with versatile functionality. The nature of the band gap is apparently dependent on the stoichiometry of biomaterial and incorporated nanomaterial. Thus we can achieve a tunable Schottky junction, based on nanomaterial dosage.

Any analyte binding is expected to change the nature of this band gap and hence the threshold. Many open hardware resources are available to develop a device that can miniaturize IV curve handling. A recent example from our group shows that chlorophyll [37] is a good sensor for nitric oxide (NO). Nitric oxide is an important determinant in a number of regulatory as well as pathophysiological processes in human, animal and plant systems. NO concentration discrimination can be done optically by studying an intrinsic fluorescence from chlorophyll. Such NO binding is expected to shift the Schottky threshold and this can be the working principle behind a sensitive, voltage based NO sensor. Voltage based sensors are cheaper and easier to handle than optical

sensors.

The capacitive properties of both biofilms and graphene-biofilm composites were expected to be sensitive to any ligand binding as described for NO. Preliminary work from our group shows that this is in fact the case and is the basis for our usage of such hybrid materials as biosensors (work in progress). Tunability of graphene dosage has resulted in the formation of sensor array, leading to even finer discrimination.

We may conceive of bioelectronic components fabricated with living bacteria. Such bio-devices would be self-powered (through H_2 production [38] and photosynthesis) and capable of self-healing in the presence of moisture and light.

Effect of graphene on photopigment concentration and growth (see Figure 5(a)) of biofilm suggests that the electron conduction properties of graphene serve to enhance energy flow through *Rhodobacter* LHC. However, this enhancement was present only when organic carbon (CH) source was abundant. Therefore we may assume that CH has a positive feedforward effect on LHC synthesis (see Supplementary, Figure S10) and functioning. Enhanced photo capture probably acts to increase the biomass of biofilms by increasing the assimilation of acquired CH from nutrient media. It may be noted that hysteresis pattern (see supplementary Figure S9) is most sensitive to the graphene-biofilm stoichiometry (as compared to capacitance decrease, which shows saturation). Further

support of graphene induced changes in biofilm morphology may be realized by the electron micrograph in absence and presence of graphene (see Figure 3).

4 Conclusions

Graphene was immobilized using live, photosynthetic biofilm and growth parameters of the biofilm changed upon such 2D material incorporation. Graphene-biofilm composite was grown on gold interdigitated electrodes and obtained IV curve exhibited a threshold above which current conduction increased rapidly. Presence of threshold indicated opening up of the band gap in graphene, as a result of immobilization, and consequent Schottky junction formation on a gold electrode. Capacitance spectrum on frequency axis revealed the presence of isosbestic points when the amplitude of AC voltage was varied.

Materials and Methods

4.1 Biocomposite synthesis

The non-sulphur bacterium belonging to Rhodobacterial species was obtained as a gift from Dr. Patrick Hallenbach, University of Montreal. The growth medium used was yeast extract supplemented RCV medium (0.3 g/L yeast extract, 4 g/L malic Acid, 1 g/L ammonium chloride, 75 mg/L calcium Chloride, 1 mg/L nicotinic acid, 20 mg/L di-sodium EDTA, 120 mg magnesium chloride, 10 mM phosphate buffer at pH 6.8).

CVD synthesized graphene was provided by commercial manufacturers in powder form (Quantum Materials Corporation, Bangalore, AzoNano, UK).

Graphene was immobilized within biofilms by a one-pot method where the (IDEs) interdigitated gold electrodes [39], on glass were submerged in the bacterial media, graphene and inoculum was added to the same and anaerobic growth was allowed to take place for 4 days, in presence of light (figures 2(a)-(g)). Graphene-biofilm composites grew as a continuous thick layer that extended over the metal electrodes as well as in the channel between two such electrodes, on the glass surface (insulator) (see figure 2).

Graphene powder was directly added to the culture medium inoculated with RCSB and biofilm growth was allowed to take place. Conditions for growth were: in transparent falcon tubes, kept up-right with no shaking, at room temperature and in presence of light. Bacterial growth with graphene was typically monitored for 4 days. For imaging purpose however, biofilms grown for 11 days was taken. Please note that graphene powder was added to growth medium without any prior dispersion in organic solvents or acid. Control samples, without added graphene, were grown in identical conditions.

Graphene incorporated biofilm grew on the wall of the falcon tubes. Graphene was initially immiscible in the aqueous RCV medium and the black mass precipitated to the bottom of the falcon tube. With biofilm formation and secretion of surfactants (apparent from increased soapy frothing) over the course of 4 days of growth, the black mass became comparatively more dispersed in the medium. Biofilm formed with the addition of graphene was blackish red and the black tint was most apparent at the bottom of the falcon tube, with film near the top of the tube being the least blackened (see figure 2 a,b and g).

Graphene incorporated biofilms were grown by adding 2 (g2), 3.3(g3), 4.4 (g4) and 5.5 mg (g5) of graphene to 50 ml media. Films were grown on bare glass cover-slips, inter-digitated gold electrodes (IDEs) on glass substrates or on aluminium foils by inserting them (see figure 2(c-f)) within the falcon tubes where biofilm growth was done. The cover-slip/foil/IDE remained completely immersed in the growth medium.

4.2 Scanning electron microscopy

SEM imaging: SEM images were obtained (see figure 2h)for samples grown on either bare coverslips or aluminium foils wrapped on glass cover-slips. SEM images were obtained with a scanning electron microscope (Model ZEISS EVO-MA 10) upgraded for imaging with biological samples. Images were obtained either with or without gold sputtering on top of either fixed or unfixed samples washed with milliQ water and dried at 50C overnight. Fixation was done with 2.5 % glutaraldehyde, washed, stained with 1 % osmium tetroxide, washed with milliQ then dehydrated in graded alcohol.

4.3 Raman spectroscopy

Raman spectrum of the graphene powder was obtained by dispersing the graphene powder in chloroform and casting a drop on quartz substrate. The Raman measurements were performed using a micro Raman set-up consisting of a spectrometer (Lab RAM HR Jovin Yvon) and a Peltier cold CCD detector. An air-cooled Argon-ion laser (Ar+) with a wavelength of 632 nm as an excitation light source. The laser was focused on the sample using 10X objective with a numerical aperture (NA) of 0.9. Power below 1 mW was used to avoid heating effect with 30 second integration
time.

4.4 FTIR spectroscopy

FTIR spectroscopy was performed by mixing sample into a KBr pellet and spectra were obtained using a Perkin Elmer FTIR spectrophotometer (Spectrum Two).

4.5 Biofilm formation assays

Biofilm formation on electrodes or cover-slip surfaces was confirmed by washing the IDEs (with biofilm grown on top) with distilled water and then observing them under a light microscope. Figure 3(a) shows an IDE with control biofilm, i.e. without graphene. Figures 3 (b and c) respectively represent the fully grown and partially peeled biofilm layer in presence of graphene. Photographs were taken of the IDEs with biofilm grown on top (see Supplementary Figure S1).

Biofilm formation on the wall of each falcon tube was quantified by two methods.

- Pigment estimation: For pigment extraction, falcon tubes with biofilm grown on their walls was washed with milliQ to remove any adhering planktonic cells, followed by treatment with 1:4 solution of chloroform and ethanol, without disrupting the adhered biofilm. Whole volume of falcon tubes was filled with organic medium and closed tubes were kept at 50 C for 45 minutes. The organic extract was collected without disrupting the attached biofilm. The absorption spectrum for each organic extract was measured in a spectrophotometer (Thermo Scientific, Model Evolution 300).

- Crystal violet staining [40]: Biofilm biomass was measured by first washing falcon tubes carefully to remove any adherent planktonic cells. After washing, whole falcon tubes were filled with 0.1% crystal violet in water, kept for 15 mins, then the staining solution was removed and washed with water to remove excess dye. The absorbed stain was extracted by treating the stained biofilms with 30% acetic acid, and the absorbance of this extract was measured at 595 nm.

Control and graphene containing samples were grown and organic extract from biofilm adhered to falcon tube walls on 2nd, 3rd and 4th days of growth and absorbance at 370 nm was
monitored.

4.6 Effect of carbon source withdrawal

Rhodobacter was grown in a semi-synthetic medium where malic acid (4 mg/ml) was the major source of organic i.e. fixed carbon. To test whether graphene acts as alternative carbon source for *Rhodobacter*, biofilms were grown in various lesser (< 4 mg/ml) concentrations as well as in absence of malic acid (i.e. 0 mg/ml). Growth was allowed either in absence or presence of graphene.

4.7 Interdigitated electrode (IDEs) fabrication

Two independent sets of IDEs were used for measurement. The capacitance measurements were performed with IDE1 fabricated in our laboratory (gap=20 μm),and the I-V measurements were performed with IDE2 (gap=10 μm), commercially procured.

IDE1 fabrication Glass substrates were first cleaned using Trichloroethylene, Acetone, Isopropyl alcohol and deionized water. They were subsequently outgassed in a vacuum chamber at 120 C. Thin films of Chromium and Gold were successively deposited using resistive heating techniques. Electrodes with 20 μm spacing were subsequently fabricated by standard photolithography and wet chemical etching processes using a solution of KI and iodine in water for gold and dilute HCl for chromium. Cover-slips containing electrodes were further cleaned with isopropyl alcohol and sterilized with 70 % alcohol and air dried in laminar air flow. Biofilms were grown by immersing these cover-slips in bacterial media during growth. Device dimensions were: 3X2 digits, dimensions: 0.2 mm X 0.16 mm, gap=20 μm.

IDE2 A second set of interdigitated electrodes were purchased from commercial manufacturers Dropsens (IDEAU10) having cell constant=0.0118 cm-1, number of digits: 125 x 2, a digit length= 6.76 mm and gap 10 μm. This arrangement was important to achieve sufficient current for measurement.

4.8 Electrical measurements

Electrical characterizations, with DC (current-voltage measurements) and AC (capacitance measurements), were done by contacting gold probes (Probe Station, Cascade Microtech) onto two inter-digitated gold electrodes by piercing through the biofilm grown on top. Hence all measurements are for current flow across the channel ((see figure 2 c, d, e and f). A two-probe system was used where one probe was earthed. The probes were connected to Keithley 4200-SCS Semiconductor Characterization System for performing measurements. For these measurements live biofilms (controls or containing graphene) were used. I-V curves were obtained by ramping voltage over various ranges and using various graphene biofilm stoichiometry. The following enlists the different conditions under which the electrical measurements were performed:

- All reading in log scale Figure (see supplementary figure S8)
- from -5 V to 5 V and back in quiet mode (IDE2, control biofilm, Figure (6)a)
- from -10 V to 10 V and back in quiet mode (IDE2, 2 mg graphene+biofilm, Figure (6)b)
- from -5 V to 5V and back in quiet mode (IDE2, 4.4 mg graphene+biofilm, Figure (6)c)

- from -1 V to 1 V and back in quiet mode (IDE2, 4.4 mg graphene+biofilm, Figure supplementary S10
- from -6V to 6 V and back in quiet mode (IDE2, 2 mg graphene+biofilm), Figure (see figure

  6(b))

Quiet mode refers to instrumental settings that control data acquisition time. Fast or quiet mode of data acquisition determines dV/dt which affects capacitive current and hysteretic properties.

4.8.1 Capacitance measurements

Capacitance spectra, on frequency axis (range: from 10 KHz to 10 MHz), were measured using AC voltage. Bio-composite was found to be insensitive to any DC bias for these measurements. Root mean square (RMS) i.e. amplitude of the AC voltage was varied to obtain capacitance spectra modulation as a function of RMS voltage from 10 mV to 100 mV(instrumental limits).

Capacitance measurements were done by applying a sinusoidally oscillating voltage across the 2 electrodes. The generated current was measured and the lag and amplitude of this current were used to calculate capacitance. The frequency of the oscillation was varied. Capacitance was plotted for varying frequency. This gives the capacitance spectrum on the frequency axis.

Miscellaneous

The authors would like to thank DBT (BT/PR3957/NNT/28/659/2013) and ICMR. SR thanks CSIR-India for Senior Research Fellowship (Sanction No.: 09/(028)0875).

Author contributions

SR and ADG designed the study. SR and AB1 performed experiments. SR, ADG and HP wrote the paper. SS, AD, AB2, AD and SC contributed towards electrical measurements procedures.
SSS and AS performed the Raman measurements.

References

[1] Azeredo, J., Azevedo, N.F., Briandet, R., Cerca, N., Coenye, T., Costa, A.R., Desvaux, M.,

Di Bonaventura, G., Hebraud, M., Jaglic, Z. *et al.* (2017) Critical review on biofilm methods. *Critical reviews in microbiology*, 43 (3), 313–351.

[2] Humphries, J., Xiong, L., Liu, J., Prindle, A., Yuan, F., Arjes, H.A., Tsimring, L., and Suel, G.M. (2017) Species-independent attraction to biofilms through electrical signaling. *Cell*, 168 (1), 200–209.

[3] Komiyama, M., Yoshimoto, K., Sisido, M., and Ariga, K. (2017) Chemistry can make strict and fuzzy controls for bio-systems: Dna nanoarchitectonics and cell-macromolecular nanoarchitectonics. *Bulletin of the Chemical Society of Japan*, 90 (9), 967–1004, doi: 10.1246/bcsj.20170156.

[4] Wei, J., Zang, Z., Zhang, Y., Wang, M., Du, J., and Tang, X. (2017) Enhanced performance of light-controlled conductive switching in hybrid cuprous oxide/reduced graphene oxide (cu2o/rgo) nanocomposites. *Opt. Lett.*, 42 (5), 911–914, doi:10.1364/OL.42.000911. URL http://ol.osa.org/abstract.cfm?URI=ol-42-5-911.

[5] Khan, A.H., Ghosh, S., Pradhan, B., Dalui, A., Shrestha, L.K., Acharya, S., and Ariga, K. (2017) Two-dimensional (2d) nanomaterials towards electrochemical nanoarchitectonics in energy-related applications. *Bulletin of the Chemical Society of Japan*, 90 (6), 627–648.

[6] Abraham, J., Vasu, K.S., Williams, C.D., Gopinadhan, K., Su, Y., Cherian, C.T., Dix, J., Prestat, E., Haigh, S.J., Grigorieva, I.V. *et al.* (2017) Tunable sieving of ions using graphene oxide membranes. *Nature nanotechnology*, 12 (6), 546.

[7] Hu, W., Peng, C., Luo, W., Lv, M., Li, X., Li, D., Huang, Q., and Fan, C. (2010) Graphenebased antibacterial paper. *ACS nano*, 4 (7), 4317–4323.

[8] McCormick, A.J., Bombelli, P., Scott, A.M., Philips, A.J., Smith, A.G., Fisher, A.C., and Howe, C.J. (2011) Photosynthetic biofilms in pure culture harness solar energy in a mediatorless bio-photovoltaic cell (bpv) system. *Energy & Environmental Science*, 4 (11), 4699– 4709.

[9] Ng, F.L., Jaafar, M.M., Phang, S.M., Chan, Z., Salleh, N.A., Azmi, S.Z., Yunus, K., Fisher, A.C., and Periasamy, V. (2014) Reduced graphene oxide anodes for potential application in algae biophotovoltaic platforms. *Scientific reports*, 4, 7562.

[10] Zhuang, L., Yuan, Y., Yang, G., and Zhou, S. (2012) In situ formation of graphene/biofilm composites for enhanced oxygen reduction in biocathode microbial fuel cells. *Electrochemistry Communications*, 21, 69–72.

[11] Yuan, Y., Zhou, S., Zhao, B., Zhuang, L., and Wang, Y. (2012) Microbially-reduced graphene scaffolds to facilitate extracellular electron transfer in microbial fuel cells. *Bioresource technology*, 116, 453–458.

[12] Yong, Y.C., Yu, Y.Y., Zhang, X., and Song, H. (2014) Highly active bidirectional electron transfer by a self-assembled electroactive reduced-graphene-oxide-hybridized biofilm. *Angewandte Chemie International Edition*, 53 (17), 4480–4483.

[13] Liu, J., Qiao, Y., Guo, C.X., Lim, S., Song, H., and Li, C.M. (2012) Graphene/carbon cloth anode for high-performance mediatorless microbial fuel cells. *Bioresource technology*, 114, 275–280.

[14] Grimm, S., Schweiger, M., Eigler, S., and Zaumseil, J. (2016) High-quality reduced graphene oxide by cvd-assisted annealing. *The Journal of Physical Chemistry C*, 120 (5), 3036–3041.

[15] Reguera, G., Nevin, K.P., Nicoll, J.S., Covalla, S.F., Woodard, T.L., and Lovley, D.R. (2006) Biofilm and nanowire production leads to increased current in geobacter sulfurreducens fuel cells. *Applied and environmental microbiology*, 72 (11), 7345–7348.

[16] Sakimoto, K.K., Kornienko, N., and Yang, P. (2017) Cyborgian material design for solar fuel production: the emerging photosynthetic biohybrid systems. *Accounts of chemical research*, 50 (3), 476–481.

[17] Nigro, M.A., Faggio, G., Fedi, F., Polichetti, T., Miglietta, M.L., Massera, E., Di Francia, G., and Ricciardella, F. (2015) Cross interference effects between water and nh 3 on a sensor based on graphene/silicon schottky diode, in *AISEM Annual Conference, 2015 XVIII*, IEEE, pp. 1–4.

[18] Svensson, J. and Campbell, E.E.B. (2011) Schottky barriers in carbon nanotube-metal contacts. *Journal of Applied Physics*, 110 (11), 111101, doi:10.1063/1.3664139. URL http://dx.doi.org/10.1063/1.3664139.

[19] Malvankar, N.S., Mester, T., Tuominen, M.T., and Lovley, D.R. (2012) Supercapacitors based on c-type cytochromes using conductive nanostructured networks of living bacteria. *ChemPhysChem*, 13 (2), 463–468.

[20] He, Z. and Mansfeld, F. (2009) Exploring the use of electrochemical impedance spectroscopy (eis) in microbial fuel cell studies. *Energy & Environmental Science*, 2 (2), 215– 219.

[21] Marsili, E., Rollefson, J.B., Baron, D.B., Hozalski, R.M., and Bond, D.R. (2008) Microbial biofilm voltammetry: direct electrochemical characterization of catalytic electrode-attached biofilms. *Applied and environmental microbiology*, 74 (23),

7329–7337.

[22] Kim, T., Kang, J., Lee, J.H., and Yoon, J. (2011) Influence of attached bacteria and biofilm on double-layer capacitance during biofilm monitoring by electrochemical impedance spectroscopy. *Water research*, 45 (15), 4615–4622.

[23] Cancado, L.G., Jorio, A., Ferreira, E.M., Stavale, F., Achete, C., Capaz, R., Moutinho, M., Lombardo, A., Kulmala, T., and Ferrari, A. (2011) Quantifying defects in graphene via raman spectroscopy at different excitation energies. *Nano letters*, 11 (8), 3190–3196.

[24] Eigler, S., Dotzer, C., and Hirsch, A. (2012) Visualization of defect densities in reduced graphene oxide. *Carbon*, 50 (10), 3666–3673.

[25] Mao, S., Lu, G., Yu, K., Bo, Z., and Chen, J. (2010) Specific protein detection using thermally reduced graphene oxide sheet decorated with gold nanoparticle-antibody conjugates. *Advanced materials*, 22 (32), 3521–3526.

[26] Kaniyoor, A. and Ramaprabhu, S. (2012) A raman spectroscopic investigation of graphite oxide derived graphene. *AIP Advances*, 2 (3), 032183.

[27] Bose, A., Raja, S.O., Chowdhury, R., Nandi, S., Ray, S., Bhattacharyya, K., and DASGUPTA, A.K. (2017) Switchable amplification of fluoresence from a photosynthetic microbe. *bioRxiv*, p. 167122.

[28] Wilking, J.N., Angelini, T.E., Seminara, A., Brenner, M.P., and Weitz, D.A. (2011) Biofilms as complex fluids. *MRS bulletin*, 36 (05), 385–391.

[29] Tu, Y., Lv, M., Xiu, P., Huynh, T., Zhang, M., Castelli, M., Liu, Z., Huang, Q., Fan, C., Fang, H. *et al.* (2013) Destructive extraction of phospholipids from escherichia coli membranes by graphene nanosheets. *Nature nanotechnology*, 8 (8), 594–601.

[30] King, A.A., Hanus, M.J., Harris, A.T., and Minett, A.I. (2014) Nanocarbon-chlorophyll hybrids: Self assembly and photoresponse. *Carbon*, 80, 746 – 754, doi:https://doi.org/10. 1016/j.carbon.2014.09.024. URL http://www.sciencedirect.com/science/ article/pii/S0008622314008768.

[31] Das, D., Sarkar Manna, J., and Mitra, M.K. (2015) Electron donating chlorophyll-a on graphene: A way toward tuning fermi velocity in an extended molecular framework of graphene/chlorophyll-a nanohybrid. *The Journal of Physical Chemistry C*, 119 (13), 6939–
6946, doi:10.1021/jp511495z. URL https://doi.org/10.1021/jp511495z.

[32] Chen, S.Y., Lu, Y.Y., Shih, F.Y., Ho, P.H., Chen, Y.F., Chen, C.W., Chen, Y.T., and Wang, W.H. (2013) Biologically inspired graphene-chlorophyll phototransistors with high gain. *Carbon*, 63, 23 – 29, doi:https://doi.org/10.1016/j.carbon.2013.06.031. URL http:// www.sciencedirect.com/science/article/pii/S000862231300540X.

[33] Heinz, H. and Ramezani-Dakhel, H. (2016) Simulations of inorganic–bioorganic interfaces to discover new materials: insights, comparisons to experiment, challenges, and opportunities. *Chemical Society Reviews*, 45 (2), 412–448.

[34] Pramanik, C., Gissinger, J.R., Kumar, S., and Heinz, H. (2017) Carbon nanotube dispersion in solvents and polymer solutions: Mechanisms, assembly, and preferences. *ACS Nano*, 11 (12), 12805–12816, doi:10.1021/acsnano.7b07684. URL https://doi.org/10.
1021/acsnano.7b07684, pMID: 29179536.

[35] Chen, J., Zhou, G., Chen, L., Wang, Y., Wang, X., and Zeng, S. (2016) Interaction of graphene and its oxide with lipid membrane: A molecular dynamics simulation study. *The Journal of Physical Chemistry C*, 120 (11), 6225–6231, doi:10.1021/acs.jpcc.5b10635. URL https://doi.org/10.1021/acs.jpcc.5b10635.

[36] Willems, N., Urtizberea, A., Verre, A.F., Iliut, M., Lelimousin, M., Hirtz, M., Vijayaraghavan, A., and Sansom, M.S.P. (2017) Biomimetic phospholipid membrane organization on graphene and graphene oxide surfaces: A molecular dynamics simulation study. *ACS Nano*, 11 (2), 1613–1625, doi:10.1021/acsnano.6b07352. URL https://doi.org/10.
1021/acsnano.6b07352, pMID: 28165704.

[37] Bhattacharya, A., Biswas, P., Kar, P., Roychoudhury, P., Basu, S., Ganguly, S., Ghosh, S., Panda, K., Pal, R., and Dasgupta, A.K. (2017) Nitric oxide sensing by chlorophyll a. *Analytica chimica acta*, 985, 101–113.

[38] Keskin, T. and Hallenbeck, P.C. (2012) Enhancement of biohydrogen production by twostage systems: dark and photofermentation. pp. 313–340.

[39] Li, H. and Bashir, R. (2002) Dielectrophoretic separation and manipulation of live and heattreated cells of listeria on microfabricated devices with interdigitated electrodes. *Sensors and Actuators B: Chemical*, 86 (2), 215–221.

[40] Merritt, J.H., Kadouri, D.E., and O'Toole, G.A. (2005) Growing and analyzing static biofilms. *Current protocols in microbiology*, pp. 1B–1.

Listing of Supplemental Digital Content

S1 Photographs of IDEs with biofilm grown on surface. Left: as- symetric growth for g2 and right: uniform biofilm growth for control biofilm

S2 SEM image showing wrinkled surface of graphene platelet (bright) trapped by biofilm cells S3 Raman spectra of graphene sample dispersed in tetrahydrofu- ran and deposited on silicon wafer, obtained with 488 nm laser

S4 Raman spectra obtained with dried control biofilm and graphene incorporated biofilm on 5th day of growth.

S5 Absorbance spectra of chloroform-ethanol extract from biofilms. Shows increase in pigment concentration of biofilm containing increasing doses of graphene.

S6 Variation in absorbance and emission at 392 nm and 613 nm respectively under malic acid limited growth conditions

S7 Absorption spectra of whole plantonic suspension for control and graphene incorporated sam-

ples.

S8 Current voltage measurements for graphene containing (g2 and g4) and control sample

S10 Interplay between electrical properties of graphene and photosynthetic bacterial metabolism

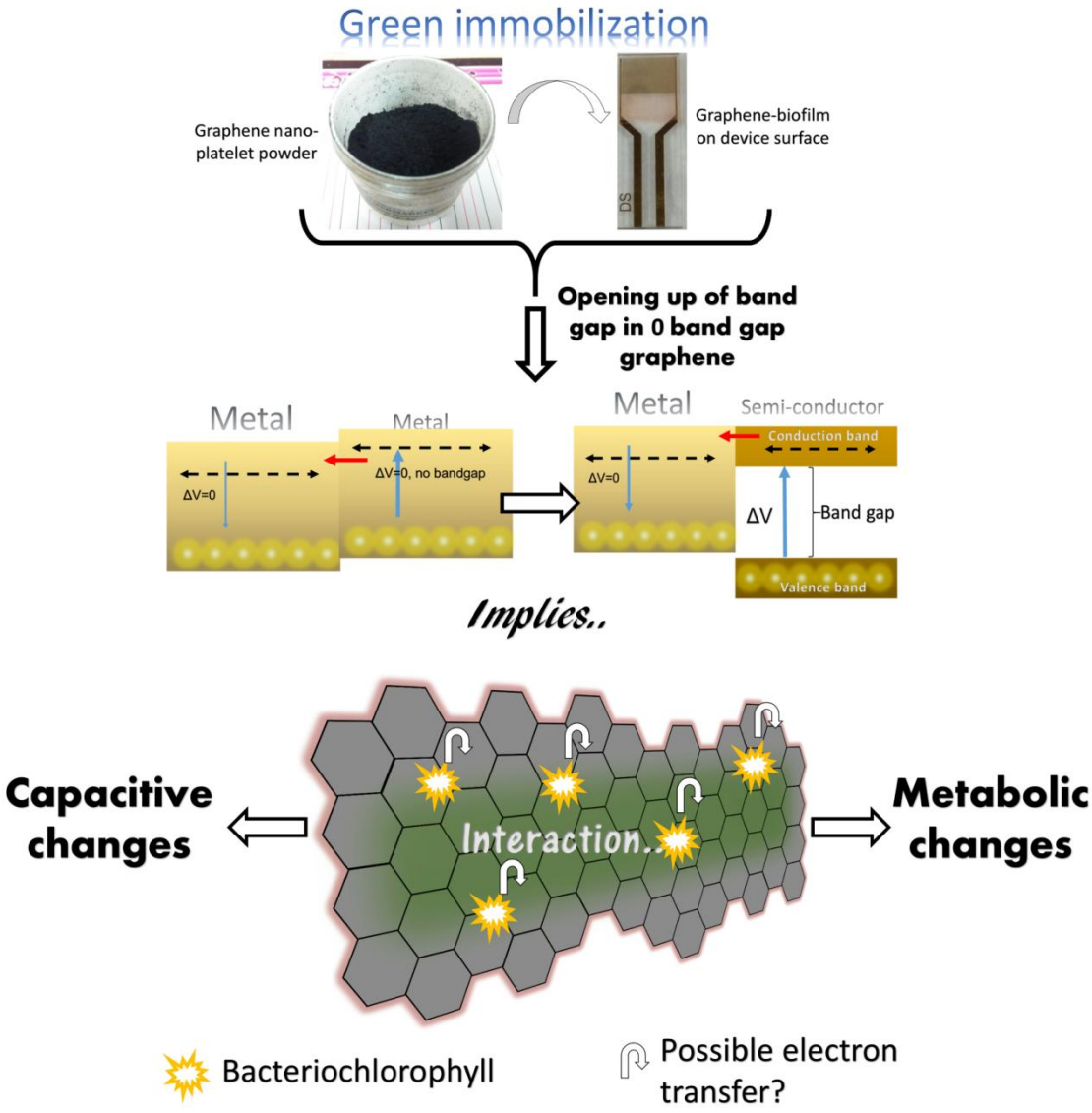

Figure 1: Outline of the work. Interaction of immobilized graphene with photosynthetic biofilm leading to emergent electrical properties as well as changes in photosynthetic metabolism.

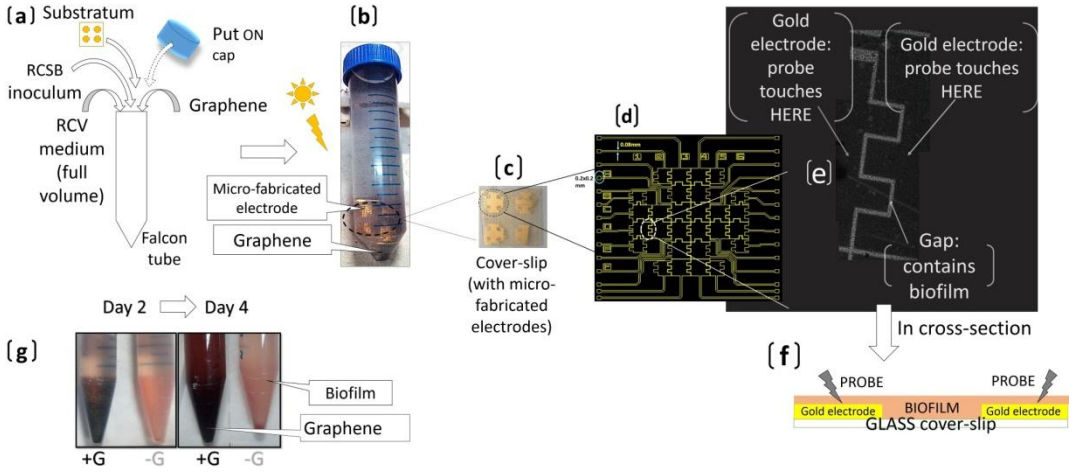

Figure 2: Synthesis of graphene-biofilm bio-composite. (a) Schematic of components added to bacterial growth medium (b) Set-up upon inoculation. (c) shows gold electrodes fabricated upon glass coverslip, 4 complexes of electrodes are present one of which is shown in Panel (d) in schematic form. Each electrode complex consists of inter-digitated electrodes with a gap of 20 micron in between (e) shows light microscopic image of micro-fabricated gold electrodes (dark area) on cover-slip with biofilm grown on top. Image obtained with lowest magnification of light microscope using 5X objective lenses, image is reconstructed from 3 overlapping micrographs of the electrode surface. The relatively lighter regions are the channels between electrodes containing no gold but with biofilm grown on the insulating substratum (glass). Panel (f) is a schematic of the same measurement set-up in cross-section.(g) Photograph of transformation of initially pristine graphene during biofilm growth

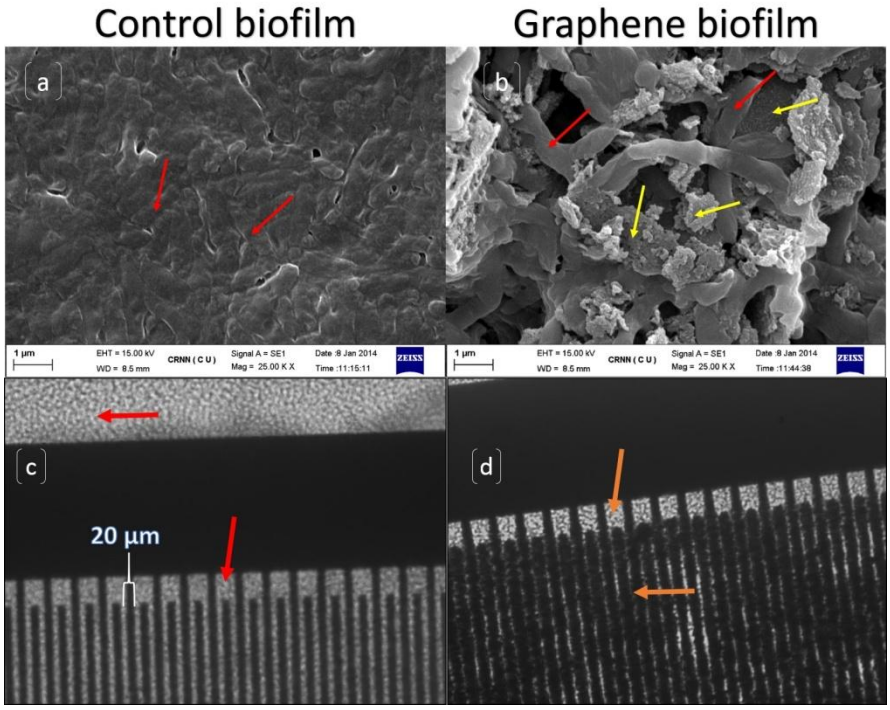

Figure 3: SEM images of (a) control biofilm (red arrows) compared to (b) graphene (yellow arrows) trapped by biofilm cells (red arrows) (c) Bright field microscopic images at 20X show an IDE with control biofilm, i.e. without graphene. (finger width is 20 μm)(d) shows fully grown biofilm with incorporated graphene. Red arrows mark biofilm cells, orange arrows mark graphene incorporated composite.

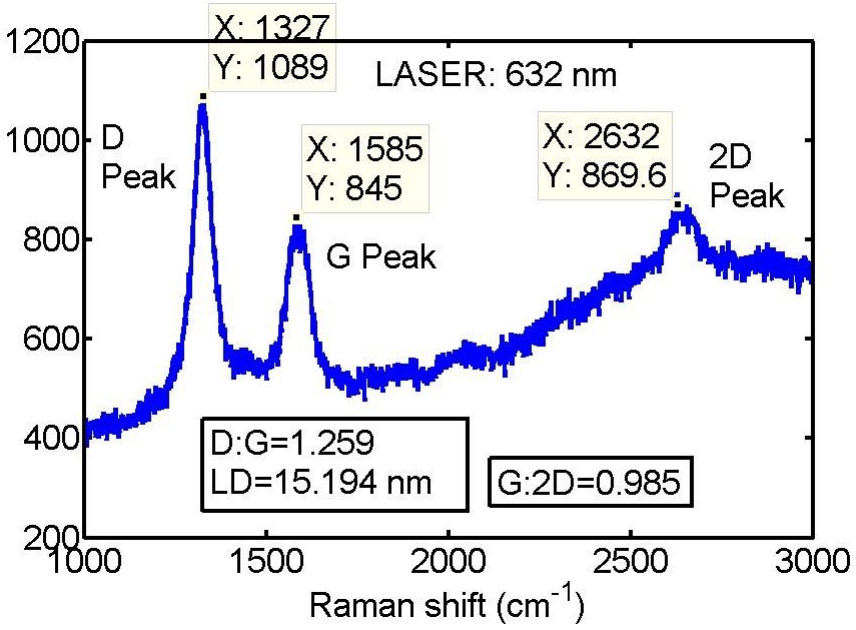

Figure 4: Raman spectrum of the graphene used in these experiments, obtained with red laser (632 nm). $I_D : I_G$ ratio was 1.259, and corresponds to L_D = 15.194 nm. 2D peak obtained showed a hump. FWHM was much greater than is typical for monolayered graphene. These features have been previously described for few layered wrinkled graphene.

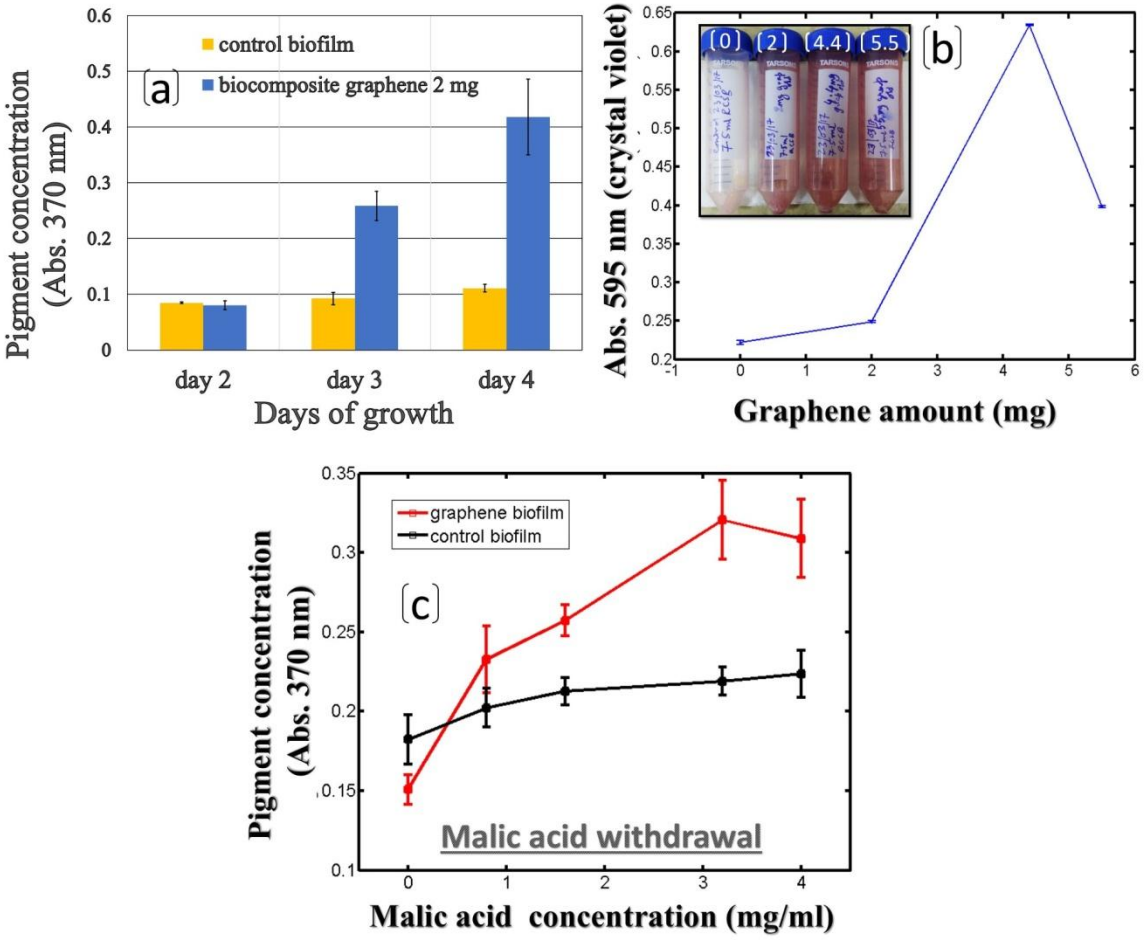

Figure 5: Biofilm characterization by standard methods and the effects of graphene incorporation (a) Change in absorbance at 370 nm of organic extract of graphene-biofilm composite (2 mg graphene in 15 ml media) compared to Rhodobacter biofilm over 2-4 days of biofilm growth. Estimation of pigment is given by measuring the absorption spectra for organic extract (using chloroform: ethanol= 1: 4) from biofilms. (b) Standard biofilm characterization by crystal violet assay. Variation in biofilm biomass with increasing graphene dose, estimated with crystal violet staining assay. Error bars are present. Inset shows photograph of biofilms adhered to falcon tube wall for each dose. (c) Variation in absorbance of organic extract at 370 nm for increasing concentrations of malic acid in growth medium, in presence and absence of graphene.

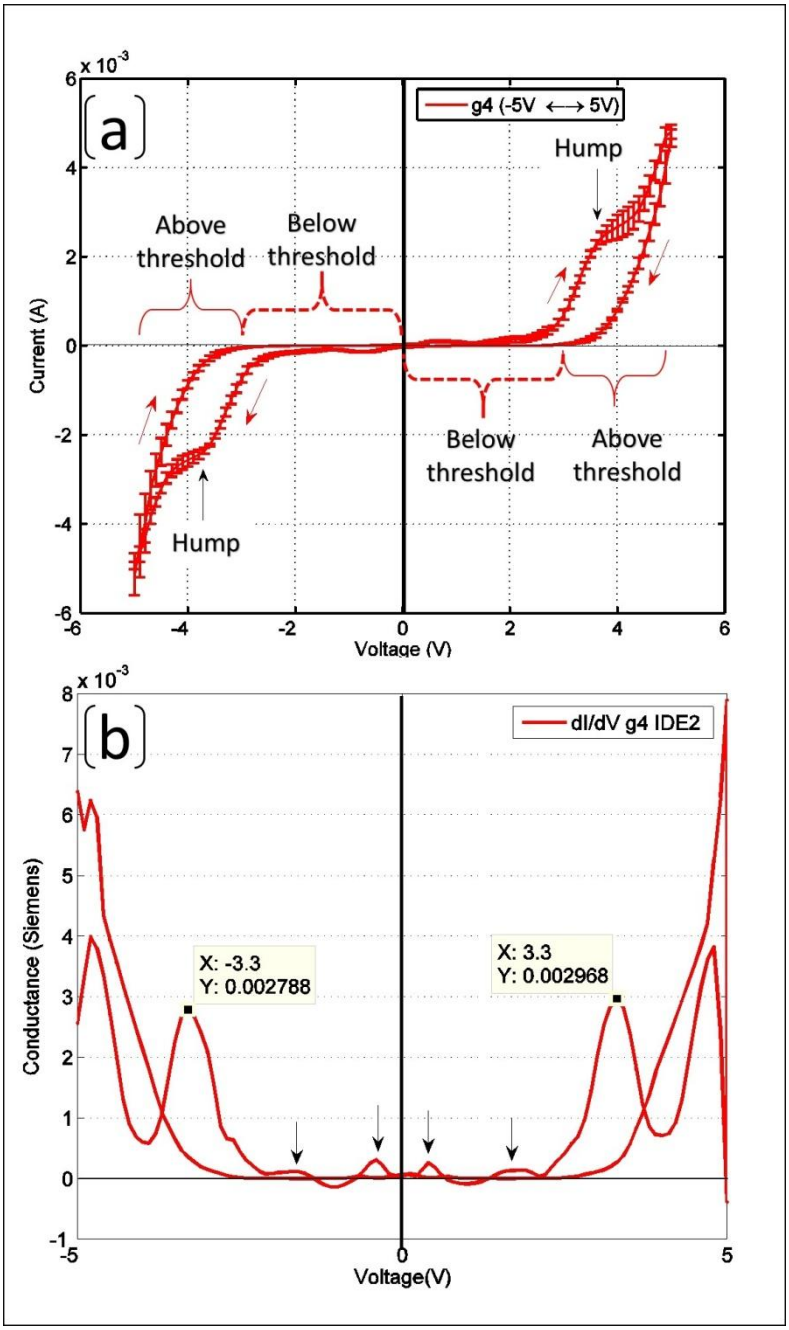

Figure 6: (a) IV curve for biofilm-graphene composite grown with 4.4 mg graphene suspended in 50 ml media (g4). Arrows indicate up or down sweep of voltage. (b) Voltage dependent conductance derived from (dI/dV) at a given V. The arrows show smaller conductance peaks along with the prominent peak at $|V| = 3.3V$, dI/dV were obtained using mean current values.

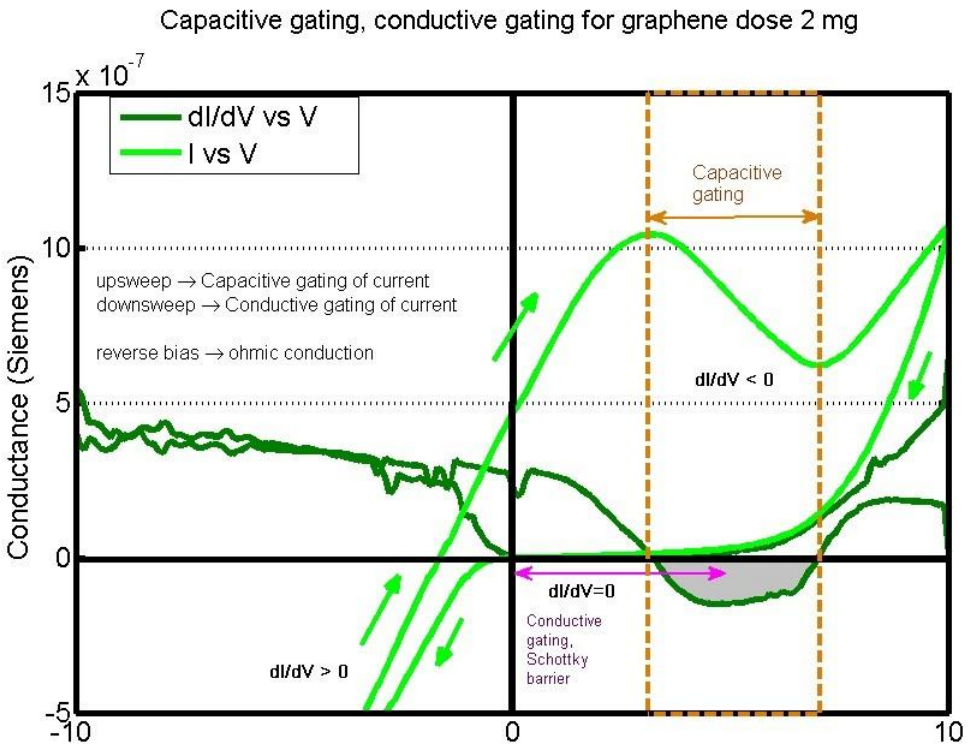

Figure 7: Current voltage curve for g2, overlayed with dI/dV versus voltage. Shows conductive gating and capacitive gating. Mean values of current were used.

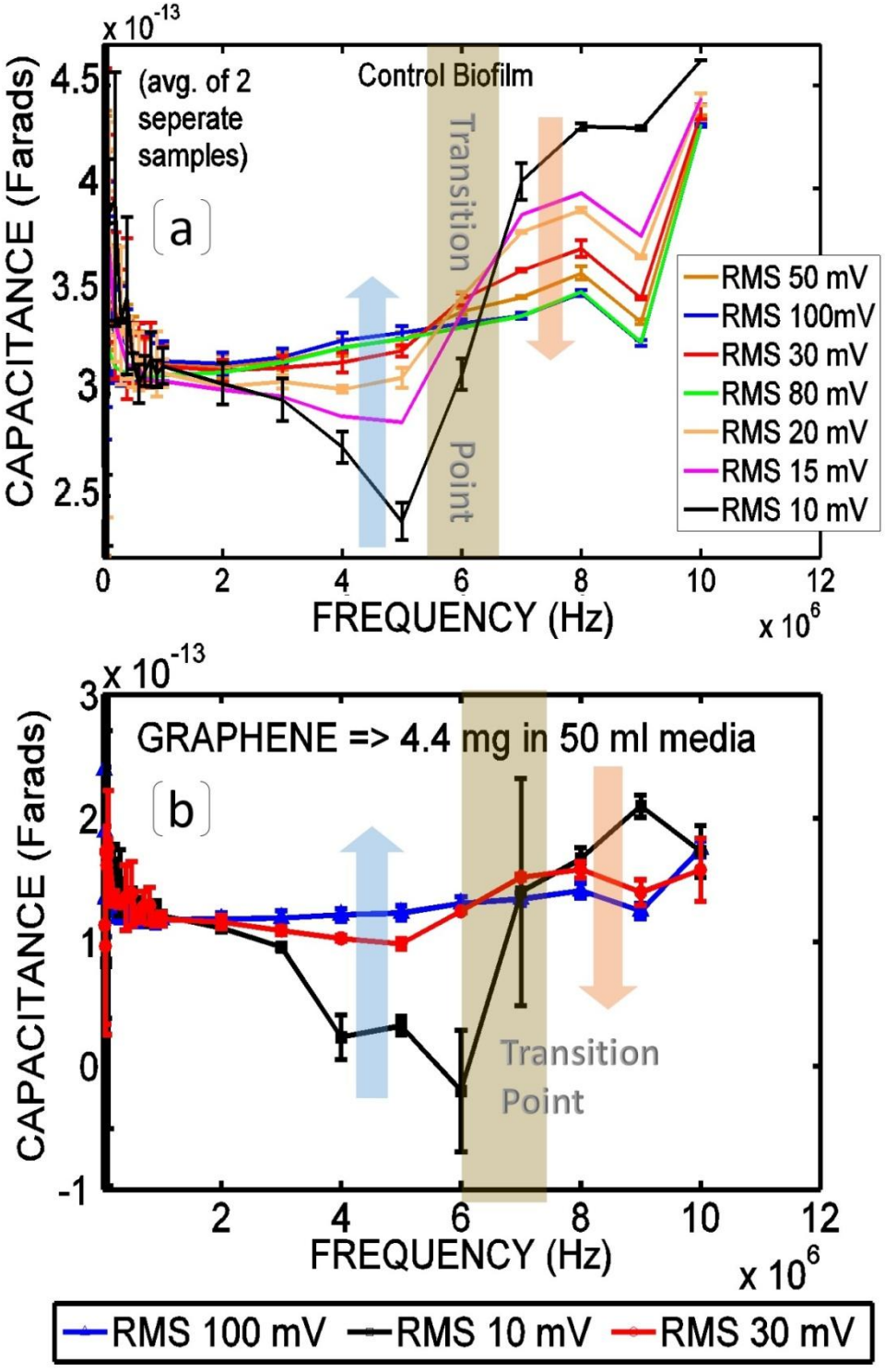

Figure 8: (a) Capacitance profiles of control biofilm. A transition point was obtained (marked a grey zone © in figure) such that capacitance increased with RMS (from 10 to 100 mV) on one side (blue arrow) and decreased with RMS on the other side (orange arrow). (b) Capacitance spectra of bio-composites (at RMS 10, 30 and 100 mV) for graphene (4.4 mg) added to 50 ml media.